Monthly Notices
of the
ROYAL ASTRONOMICAL SOCIETY

Mon. Not. R. Astron. Soc. **413,** 2339–2344 (2011) doi:10.1111/j.1365-2966.2011.18297.x

Discovery of the new class I methanol maser transition at 23.4 GHz

M. A. Voronkov,[1,2★] A. J. Walsh,[3] J. L. Caswell,[1] S. P. Ellingsen,[4] S. L. Breen,[1,4] S. N. Longmore,[5] C. R. Purcell[6] and J. S. Urquhart[1]

[1]*Australia Telescope National Facility, CSIRO Astronomy and Space Science, PO Box 76, Epping, NSW 1710, Australia*
[2]*Astro Space Centre, Profsoyuznaya st 84/32, 117997 Moscow, Russia*
[3]*Centre for Astronomy, School of Engineering and Physical Sciences, James Cook University, Townsville, QLD 4814, Australia*
[4]*School of Mathematics and Physics, University of Tasmania, GPO Box 252-37, Hobart, Tasmania 7000, Australia*
[5]*ESO Headquarters, Karl-Schwarzschild-Str, 2, 85748 Garching bei München, Germany*
[6]*School of Physics and Astronomy, University of Leeds, Leeds LS2 9JT*

Accepted 2011 January 5. Received 2010 December 31; in original form 2010 December 1

ABSTRACT

We report the first detection of a methanol maser in the 10_1–9_2 A^- transition at 23.4 GHz, discovered during the H_2O southern Galactic Plane Survey (HOPS) with the 22-m Mopra Radio Telescope. In the region covered by HOPS, the 23.4-GHz maser was found at only one location, G357.97−0.16, which was also a prominent source of maser emission in the J_2–J_1 E series near 25 GHz. The Australia Telescope Compact Array (ATCA) was used to follow up these detections at high angular resolution and prove the maser nature of the observed emission. The analysis shows that the new methanol maser at 23.4 GHz is a class I maser, which has properties similar to the 9.9- and 25-GHz masers (i.e. traces strong shocks with higher than average temperature and density). All class I masers were found to originate at the same spatial location (within the measurement uncertainty of 0.5 arcsec) in the vicinity of the dominant infrared source, but at a clearly distinct position from nearby OH, H_2O and class II methanol masers at 6.7 GHz. All maser species are distributed approximately on a line, but it is not clear at present whether this has any physical significance. We also detected a weak (1.3 mJy) continuum source at 25 GHz near the OH maser (at the most northern site, associated with a class II methanol maser and an H_2O maser renowned for its extremely wide spread of velocity components). The continuum source has not been reported at lower frequencies and is therefore a candidate hypercompact H II region. We also used the ATCA to find the strongest and only the fifth known 9.9-GHz maser towards G357.97−0.16 and another 23.4-GHz maser towards G343.12−0.06 not seen in HOPS.

Key words: masers – ISM: molecules.

1 INTRODUCTION

Methanol masers are associated with regions of active star formation, with more than 20 different centimetre and millimetre wavelength maser transitions discovered to date (e.g. Müller, Menten & Mäder 2004). There are two distinct classes of methanol masers as suggested empirically in the early studies (Batrla et al. 1987). Widespread class I masers such as 44- and 95-GHz masers usually occur in multiple locations across the star-forming region scattered around an area up to a parsec in extent (e.g. Kurtz, Hofner & Álvarez 2004; Voronkov et al. 2006; Cyganowski et al. 2009). In contrast, class II methanol masers (e.g. at 6.7 and 12 GHz), along with OH and H_2O masers, reside in the close vicinity of exciting young stellar objects (YSOs) and are typically found as a single cluster of emission at arcsecond resolution (e.g. Caswell et al. 2010).

Theoretical calculations can explain this empirical classification and strongly suggest that the pumping process of class I masers is dominated by collisions with molecular hydrogen, in contrast to class II masers which are pumped by radiative excitation (e.g. Cragg et al. 1992). The two pumping mechanisms were shown to be competitive (for an illustration, see Voronkov et al. 2005): strong radiation from a nearby infrared source quenches class I masers and increases the strength of class II masers. Therefore, bright masers of different classes residing in the same volume of gas are widely accepted as mutually exclusive (note that there could be exceptions for weak masers). However, on larger scales, they are often observed to coexist in the same star-forming region within less than a parsec of each other. The exceptions are a few archetypal sources where only one particular class of methanol masers has been detected.

★E-mail: Maxim.Voronkov@csiro.au

The class I methanol masers are less studied than the class II counterparts but have recently become a subject of intense research. The common consensus is that class I masers trace shocked gas, where the conditions favour collisional excitation and a significant amount of methanol is released from dust grain mantles. The exact physical phenomena causing shocks traced by masers probably vary from source to source (see, e.g. Voronkov et al. 2010, and references therein) although for most of these masers, the shocks probably arise from an interaction between outflows and the ambient molecular material (e.g. Plambeck & Menten 1990; Kurtz et al. 2004; Voronkov et al. 2006; Cyganowski et al. 2009).

In addition to the gross classification, there are finer distinctions within the same class of methanol maser transitions. At sub-Jy sensitivity levels, the range of transitions can be further categorized into widespread masers and rare or weak masers. For example, more than 100 maser sources are known at 44 GHz (e.g. Haschick, Menten & Baan 1990; Slysh et al. 1994; Cyganowski et al. 2009), while very few were found at 9.9 GHz despite a sensitive search towards a large number of targets (Voronkov et al. 2010). Another example of rarer masers is the J_2–J_1 E series near 25 GHz. Historically, these were the first methanol masers found in space (Barrett, Schwartz & Waters 1971; Hills, Pankonin & Landecker 1975), but were believed to be rare following the survey of Menten et al. (1986). However, it has recently been shown by a more sensitive survey that the 25-GHz masers are quite common but weak (typically weaker than 1 Jy; Voronkov et al. 2007). The modelling to date suggests that class I masers at 9.9 GHz and the series of masers near 25 GHz require higher temperatures and densities to form than their widespread counterparts (Sobolev et al. 2005). This is in agreement with the less frequent appearance of these masers. In this paper, we present the first detection of a new class I methanol maser at 23.4 GHz, which shows similar properties to 9.9- and 25-GHz masers and may shed light on class I methanol maser origins.

2 OBSERVATIONS

The initial detection of the 10_1–9_2 A$^-$ methanol maser at 23.4 GHz was made as part of the H_2O southern Galactic Plane Survey (HOPS; see also Walsh et al. 2008) towards a single location G357.97−0.16. HOPS is an unbiased survey of the southern Galactic plane at frequencies between 19.5 and 27.5 GHz, carried out using the Mopra Radio Telescope. It was designed primarily to detect water masers and NH_3 emission, but it also covered a range of methanol maser transitions of both class I and class II. The zoom mode of the Mopra Spectrometer (MOPS) was used in the survey. It provided 16 simultaneous spectral windows, each 137.5-MHz wide and split into 4096 channels, positioned within the 8.3-GHz-wide receiver band around the frequencies of interest. The attained spectral resolution varied with frequency from 0.3 to 0.5 km s^{-1}. HOPS has covered 100 deg^2 of the Galactic plane between the longitudes 290° and 30° through the Galactic Centre and latitudes ±0.°5 with the typical 1σ noise level of around 1–2 Jy. It is worth noting, however, that a high signal-to-noise ratio is required to detect masers (at least 5σ, if not more) because the spectral resolution of HOPS is relatively coarse and the masers are expected to appear as single channel spikes. Further details on the survey will be published in a technique paper (Walsh et al., in preparation).

The HOPS detection of the 23.4-GHz maser and the J_2–J_1 E maser series near 25 GHz towards G357.97−0.16 was followed up with the Australia Telescope Compact Array (ATCA) on 2010 June 19 (project code CX110) using the recently commissioned zoom modes of the Compact Array Broadband Backend (CABB), which allowed us to observe eight maser transitions simultaneously. In addition to this, we searched for another rare methanol maser at 9.9 GHz towards this source in a separate observation on June 7. The full list of observed transitions is given in Table 1 along with the rest frequency for each transition, corresponding velocity uncertainty and observed velocity range. The majority of rest frequencies were taken from Müller et al. (2004). However, we adopted an astronomical measurement of the rest frequency for the 9.9-GHz transition (Voronkov et al. 2006). It agrees with the laboratory measurement of Müller et al. (2004), which has the uncertainty of 0.12 km s^{-1}. The rest frequency for the 23.4-GHz transition was taken from Mehrotra, Dreizler & Mäder (1985).

Table 1. Methanol maser transitions observed with ATCA.

Molecular transition	Rest frequency (MHz)	Rest frequency uncertainty (MHz)	(km s^{-1})	Velocity range (km s^{-1})
		2010 June 19		
2_2–2_1 E	24 934.382	0.005	0.060	−9.3, 0.8
3_2–3_1 E	24 928.707	0.007	0.084	−11.5, −1.2
4_2–4_1 E	24 933.468	0.002	0.024	−8.3, 2.0
5_2–5_1 E	24 959.0789	0.0004	0.005	−6.9, 3.3
6_2–6_1 E	25 018.1225	0.0004	0.005	−12.2, −2.1
7_2–7_1 E	25 124.8719	0.0004	0.005	−9.4, 0.9
8_2–8_1 E	25 294.4165	0.0004	0.005	−8.8, 1.5
10_1–9_2 A$^-$	23 444.778	0.002	0.026	−11.9, −0.9
		2010 7 June		
9_{-1}–8_{-2} E	9936.201	0.001	0.030	−22.7, 4.5

The correlator split each 1-MHz-wide zoom window into 2048 spectral channels providing a spectral resolution of about 0.015 and 0.006 km s^{-1} for the 9.9 and 23–25 GHz observing sessions, respectively. In addition, two 2-GHz-wide windows with 1-MHz spectral resolution were also available for simultaneous continuum measurement. These broad-band windows were set to overlap in order to accommodate the particular configuration of zoom windows used for the spectral line observations. This set-up provided an effective bandwidth of 3 GHz (the overlap region does not improve the signal-to-noise ratio).

The ATCA antennas were in an extended 6C array configuration for both observing slots giving baselines ranging from 153 m up to 6 km.[1] Note, however, that CA02 antenna forming the shortest baseline of the 6C configuration was not available during the 23–25 GHz observations on June 19 (the second shortest baseline was 413 m). Both observing slots were short (6 h on June 19 and just 30 min on June 7), resulting in an asymmetric synthesized beam of about 1.3 × 0.3 arcsec at a position angle of −38° for the 23–25 GHz transitions and precluding any imaging at 9.9 GHz. For the latter, we performed phase-only self-calibration with a solution interval of 3 min and assumed a point source model at the position of the strongest component of the 23.4-GHz maser (see the following section) to extract the spectrum.

The position of the phase and pointing centre was $\alpha_{2000} = 17^h41^m19^s.12$, $\delta_{2000} = -30°44'58''.06$ for both observing slots. For the June 19 slot, we used reference pointing procedures and determined corrections using the continuum source 1714−336 (which served also as a phase calibrator). From the statistics of the pointing solutions, the reference pointing accuracy was estimated to be 2.6 ± 2.2 arcsec. The 9.9-GHz observations were done using the

[1] More details on the ATCA configurations are available on the web (http://www.narrabri.atnf.csiro.au/observing/configs.html).

global pointing model which is expected to be accurate to about 10 arcsec. The primary beam size was about 2 arcmin at 23–25 GHz and 5.1 arcmin at 9.9 GHz. Note that pointing errors affect the accuracy of flux density measurements, while the accuracy of the obtained absolute positions depends primarily on the quality of the phase calibration and is believed to be better than 0.5 arcsec. At the position of the masers, which are discussed in the following section, these pointing uncertainties correspond to flux density uncertainties of 1 and 2 per cent at 9.9 and 23–25 GHz, respectively. The absolute flux density scale was bootstrapped from observations of 1934−638. We expect it to be accurate to better than 3 and 10 per cent at 9.9 and 23–25 GHz, respectively. The assumed flux densities were 2.39 and 0.75 Jy at 9.9 and 23.4 GHz, respectively.

The data reduction was performed using the MIRIAD package (CABB release) following standard procedures and ignoring wide-bandwidth effects for the continuum measurement (these effects are negligible for narrow zoom windows). Each spectral window produced by CABB was processed independently, although we merged the overlapping broad-band windows together for imaging after the calibration and removal of contaminating spectral lines. The imaging was performed for the whole field of view and used natural weighting. We searched for maser emission in the image cube prior to the primary beam correction (i.e. the noise across the field of view was constant). Then, the cube was divided by the primary beam model at the appropriate frequency, and the spectra were extracted at the peak pixel by taking a slice along the spectral axis. We followed this approach due to the rather high sidelobe level in the point spread function caused by the poor *uv*-coverage attained in the project. This method reproduces the flux density correctly in the case of unresolved or barely resolved sources (i.e. smaller than the synthesized beam) and is well suited to maser observations.

3 RESULTS

3.1 ATCA spectra of the masers

We detected emission in all class I maser transitions observed towards G357.97−0.16 (see Table 1). This is an independent confirmation of the HOPS detections. In addition, the search for the 9.9-GHz maser yielded a detection of only the fifth maser at this frequency. It has a peak flux density of around 70 Jy, exceeding that of all other known 9.9-GHz masers by an order of magnitude (cf. Voronkov et al. 2010). The spectra of all observed transitions are shown in Fig. 1. It is clear that a number of spectral components contribute to the overall profile for each transition. The relative flux densities of these components vary with transition which is reflected by the shapes of the spectra in Fig. 1 and by the slightly broader appearance of the spectral profiles corresponding to the high excitation $J = 7$ and 8 transitions of the J_2–J_1 E series in comparison to the lower J transitions. The apparent offset in velocity (most pronounced for the $J = 3$ transition) is consistent with the rest frequency uncertainty.

To analyse the profiles in detail, we decomposed the spectra into a number of Gaussian components listed in Table 2. The first column shows the molecular transition in the same order as in Fig. 1. The following five columns represent the peak velocity, absolute position (except for the 9.9-GHz components, for which no position measurement was possible), linewidth given as the full width at half-maximum (FWHM) and the flux density for every Gaussian component constituting the profile. Uncertainties are given in brackets and expressed in the units of the least significant figure. They are the formal uncertainties of the fit and do not take into account systematic effects. It is evident from Table 2 that all components of all measured transitions arise at the same location within the positional uncertainty of our measurement (about 0.5 arcsec). Therefore, the 9.9-GHz profile, which was obtained towards the same position by choice, correctly represents the strength of the different components contributing to the profile. We used the smallest number of Gaussian components required to fit the profile within the measurement errors. However, it is evident from both Table 2 and Fig. 1 that the radial velocities of components corresponding to the $J \leq 6$ transitions of the 25-GHz series are different from that of the

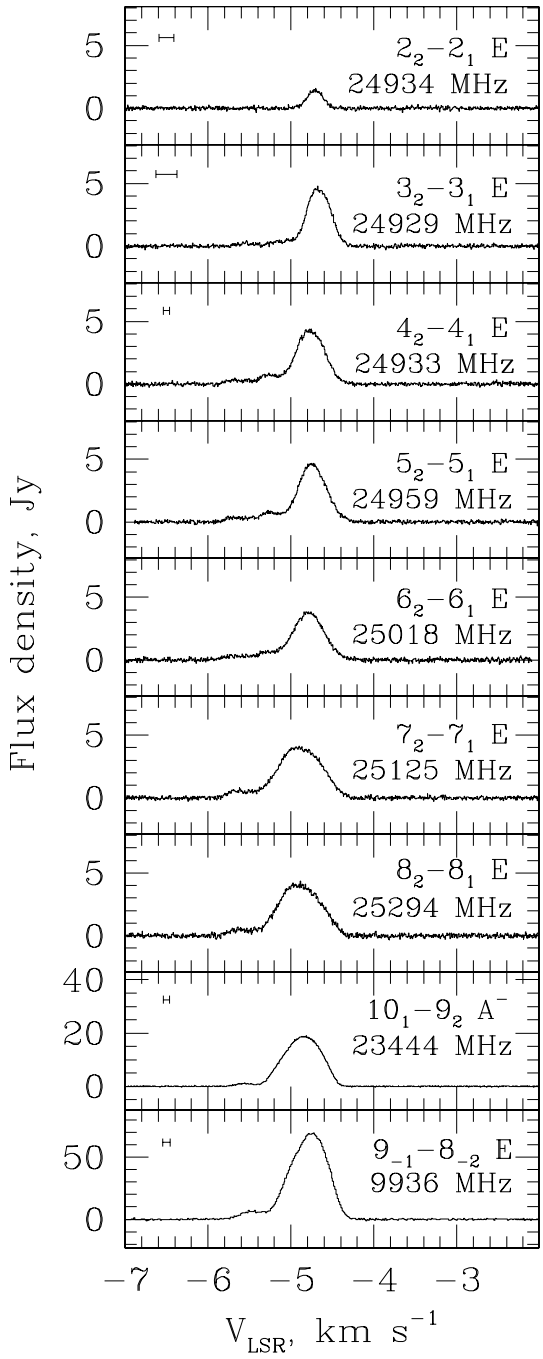

Figure 1. Spectra of the masers detected in G357.97−0.16. Horizontal error bars show the 3σ uncertainty in radial velocity caused by the rest frequency uncertainty (the error bars are only shown if the uncertainty notably exceeds the spectral resolution).

Table 2. Fit results and profile parameters. The uncertainties are given in parentheses and expressed in units of the least significant figure.

Molecular transition	Gaussian components					Peak	Peak	
	LSR[c] velocity[a] ($km\,s^{-1}$)	α_{2000} 17^h41^m (^{s})	δ_{2000} $-30°45'$ ($''$)	Line FWHM ($km\,s^{-1}$)	Flux density (Jy)	LSR[c] velocity[b] ($km\,s^{-1}$)	flux density (Jy)	$\int f(v)\,dv$ ($Jy\,km\,s^{-1}$)
2_2–2_1 E	−4.710	20.051 (6)	18.1 (1)	0.224 (4)	1.43 (2)	−4.703	1.6 (2)	0.34 (3)
3_2–3_1 E	−5.53	20.056 (8)	18.1 (1)	0.25 (3)	0.22 (2)	−4.679	4.8 (5)	1.8 (2)
	−5.14	20.067 (9)	18.4 (2)	0.25 (2)	0.39 (2)			
	−4.665	20.049 (5)	18.06 (7)	0.333 (2)	4.67 (2)			
4_2–4_1 E	−5.64	20.04 (2)	17.9 (3)	0.30 (3)	0.32 (2)	−4.756	4.4 (5)	2.1 (2)
	−5.280	20.07 (2)	18.5 (2)	0.23 (1)	0.70 (2)			
	−4.766	20.050 (4)	18.07 (6)	0.399 (2)	4.32 (2)			
5_2–5_1 E	−5.63	20.05 (1)	18.03 (2)	0.33 (3)	0.37 (2)	−4.733	4.7 (5)	2.2 (2)
	−5.265	20.064 (9)	18.3 (2)	0.24 (1)	0.74 (2)			
	−4.744	20.051 (5)	18.10 (7)	0.392 (2)	4.60 (2)			
6_2–6_1 E	−5.67	20.05 (2)	18.3 (3)	0.34 (4)	0.31 (2)	−4.757	3.8 (4)	2.0 (2)
	−5.302	20.06 (1)	18.3 (1)	0.27 (2)	0.53 (2)			
	−4.788	20.050 (6)	18.05 (7)	0.433 (3)	3.78 (2)			
7_2–7_1 E	−5.63	20.06 (1)	18.2 (2)	0.30 (2)	0.56 (2)	−4.901	4.1 (4)	2.7 (3)
	−4.95	20.050 (4)	18.06 (7)	0.50 (1)	3.87 (8)			
	−4.64	20.048 (6)	18.02 (9)	0.33 (2)	1.4 (2)			
8_2–8_1 E	−5.625	20.059 (8)	18.2 (2)	0.28 (2)	0.49 (3)	−4.886	4.3 (4)	2.6 (3)
	−4.96	20.051 (5)	18.09 (7)	0.48 (2)	3.94 (8)			
	−4.64	20.051 (8)	18.1 (1)	0.33 (2)	1.5 (2)			
10_1–9_2 A^-	−5.584	20.049 (8)	18.0 (1)	0.191 (8)	1.00 (4)	−4.814	19 (2)	11 (1)
	−4.932	20.050 (3)	18.07 (3)	0.450 (5)	16.4 (2)			
	−4.675	20.050 (3)	18.07 (5)	0.301 (4)	8.6 (4)			
9_{-1}–8_{-2} E	−5.493	No imaging		0.30 (1)	6.1 (1)	−4.73	69 (2)	40 (1)
	−4.89			0.44 (2)	50 (2)			
	−4.638			0.34 (7)	41 (4)			

[a]The fit uncertainty is half of that for the line FWHM.
[b]The uncertainty is the spectral resolution.
[c]Local standard of rest.

rest of the transitions which correspond to higher excitation energies. It is therefore likely that more than three physical components are present, but some fade away in transitions with higher excitation energies while others become brighter. The last three columns describe each measured spectral profile as a whole prior to decomposition into components. These columns are the peak velocity, the corresponding flux density and the integrated flux density over the line profile. The corresponding uncertainties of the flux density and the integral take into account the accuracy of the absolute flux scale calibration.

Astronomical observations are sometimes used to improve the accuracy to which the transition rest frequencies are known (e.g. Voronkov et al. 2006). The main drawback of this method is the assumption of equal radial velocities for different transitions, which may be misleading due to unresolved source structure and varying excitation conditions. However, it is evident from Fig. 1 and Table 2 that the spectral profiles for the $J < 6$ transitions of the 25-GHz series look very consistent. Therefore, we can refine the rest frequencies of the lower J transitions using the $J = 5$ transition as a reference. The latter has the rest frequency known to higher accuracy than the spectral resolution of our measurement (see Table 1). Assuming that the brightest Gaussian component from Table 2 peaks at the same velocity, the rest frequencies are 24 934.379 ± 0.001, 24 928.7004 ± 0.0008 and 24 933.4698 ± 0.0008 MHz, for the $J = 2$, 3 and 4 transitions of the J_2–J_1 E methanol series, respectively. The uncertainties are determined by the accuracy of the fit combined with the uncertainty of the rest frequency for the $J = 5$ transition and the spectral resolution. It is not practical to adjust the rest frequency for other transitions.

3.2 Morphology of the region

The region is a known site of water, OH and class II methanol masers at 6.7 GHz (Taylor, Morris & Schulman 1993; Caswell 1998; Breen et al. 2010; Caswell et al. 2010). The morphology of the region is shown in Fig. 2, where the positions of various masers are overlaid on the 8.0-μm image obtained with the *Spitzer Space Telescope's* Infrared Array Camera (IRAC). Inspection of other IRAC bands revealed no pronounced diffuse emission at 3.6, 4.5 and 5.8 μm similar to the diffuse structures seen at 8.0 μm (see Fig. 2). The dominant infrared source located near the position of class I masers is likely to be saturated in all IRAC bands, and therefore the emission excess at 4.5 μm, which is often regarded as a signature of shocked gas (see, e.g. De Buizer & Vacca 2010), cannot be determined. Likewise, no Extended Green Object (EGO; extended emission with an excess of flux density at 4.5 μm) has been reported in this region.

There are two distinct sites of water and 6.7-GHz methanol maser emission separated by about 8 arcsec (see Fig. 2). The southern site is located close to the dominant infrared source, while the northern maser site is located near a weak source seen only at 8.0 μm, the longest IRAC wavelength. This source is detected in 24-μm *Spitzer* observations, which means that it is most likely deeply embedded in the parent molecular cloud. The hydroxyl maser has been detected towards the northern site only (located within 2 arcsec from other masers; Caswell 1998). This OH maser has a velocity range from −10 to $-4\,km\,s^{-1}$ (Caswell 1998), while the 6.7-GHz methanol emission in the northern site is confined to radial velocities from −6 to $0\,km\,s^{-1}$. In contrast, the water maser in the northern site has

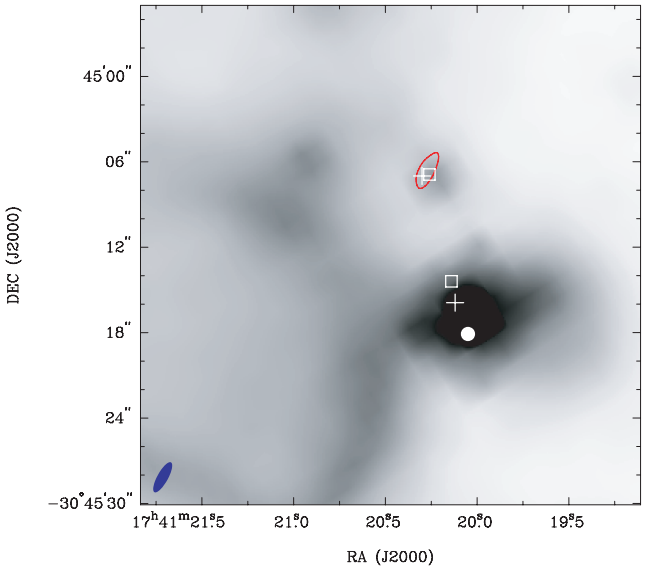

Figure 2. Position of class I methanol masers (circle), class II methanol masers at 6.7 GHz (squares) and water masers (crosses) in G357.97−0.16 overlaid on top of the 8.0-μm IRAC *Spitzer* image. The 12-mm continuum source, which has the peak flux density of 1.3 mJy at 25 GHz, is shown by a single 50 per cent contour. The ellipse in the bottom left-hand corner represents the synthesized beam of the continuum measurement.

an unusually wide spread of velocity components (about 180 km s^{-1} wide; Breen et al. 2010) and near continuous emission across the whole velocity range.

The companion water maser in the southern site shows much more modest velocity spread of about 15 km s^{-1} (Breen et al. 2010). The corresponding 6.7-GHz methanol maser is notably weaker than the maser in the northern site (approximately 3 Jy versus 50 Jy in the northern site; Caswell et al. 2010), but has a slightly wider velocity spread from −9 to +3 km s^{-1}. The class I methanol masers are located a few arcseconds offset from the southern site of water and class II methanol masers (near the opposite edge of the brightest infrared peak, see Fig. 2). Their radial velocities, which are typically found close to the systemic velocity (see e.g. Voronkov et al. 2006), are near −5 km s^{-1} (see Table 2) and fall within the velocity interval of the class II maser. Despite the fact that this source is observed in the general direction of the Galactic Centre, the kinematics do not allow us to make a definite association. With the systemic velocity around −5 km s^{-1}, the distance to this source is highly uncertain (see also the discussion in Caswell et al. 2010).

It is worth noting that the class I masers are located approximately on the extension of the line joining the northern and southern maser sites. However, the available data on the source do not allow us to establish whether these sites of maser emission are somehow physically related (e.g. trace a common outflow). It is also not clear whether there is a connection between an unusual water maser in the northern site and the rare class I methanol maser in the southern site. Interferometric observations of the widespread class I methanol masers (such as masers at 36 and 44 GHz) towards this source are likely to shed light on this question. These masers often consist of numerous spots aligned in a regular structure, which presumably traces shocks, and, therefore, have a high potential to reveal an outflow (e.g. Kurtz et al. 2004; Voronkov et al. 2006; Cyganowski et al. 2009).

The complementary continuum measurement yielded the detection of a weak (peak flux density is 1.3 ± 0.4 mJy beam^{-1} at 25 GHz) compact source near the northern group of masers (Fig. 2). The present data do not allow us to estimate the spectral index with sufficient accuracy to be able to constrain emission models. The source appears to be very slightly resolved although observations with a better *uv*-coverage are required to confirm this. This is the first detection of a radio continuum source towards this position. The source is more than an order of magnitude weaker than the continuum detection limit of Breen et al. (2010). It remained undetected in the 5-GHz survey of Becker et al. (1994) with a flux density limit of around 2.5 mJy. Therefore, this continuum source is a good candidate to be a hypercompact H II region although the present low frequency flux density limit does not allow us to rule out other possibilities like a jet, stellar wind or an ultracompact H II region.

4 DISCUSSION

The 10_1–9_2 A$^-$ methanol transition at 23.4 GHz was first observed in absorption towards an archetypal class II methanol maser source W3(OH) by Menten et al. (1985). This fact alone suggests that the maser in this transition should belong to class I. This is because the maser pumping influences level populations in the opposite way for the strong maser transitions of different classes (for details see fig. 5 and the associated discussion in Voronkov et al. 2005), which can sometimes lead to absorption. It is also worth noting that Sobolev et al. (2007) conducted sensitive observations of 20 targets at 23.4 GHz as part of their search for the 23.1-GHz class II methanol masers. No emission at 23.4 GHz was detected towards the sources where the class II maser was also found. The attribution of the 23.4-GHz masers to class I is corroborated by the pumping models of Cragg et al. (1992), which predicted these masers when collisional transitions dominate (i.e. the case of class I masers). The methanol emission in G357.97−0.16 was found to be unresolved for all observed transitions, despite using the most extended array configuration of ATCA. This implies the brightness temperature is in excess of 10^6 K and confirms the maser nature of the observed emission. This conclusion is further reinforced by the narrow width of the spectral profiles (see Fig. 1 and Table 2). The 23.4-GHz maser was found to coincide spatially within the measurement uncertainty with the 25-GHz masers, a well established class I methanol maser series (see, e.g. Voronkov et al. 2005). All these facts along with the detection of a rare class I methanol maser at 9.9 GHz leave no doubt that the 23.4-GHz maser we found towards G357.97−0.16 also belongs to the same class. Moreover, analogous to the 9.9-GHz and bright 25-GHz masers, the 23.4-GHz masers are likely to originate from the areas with the most prominent interaction between shocks and quiescent medium, resulting in higher than average temperatures and densities. It is not clear at present whether 23.4-GHz masers are as rare as the 9.9-GHz ones (see Voronkov et al. 2010) or are weak and common as the 25-GHz masers (see Voronkov et al. 2007). Note that the sensitivity and the spectral resolution attained in HOPS allowed us to detect the strongest masers only. The survey sensitivity was suited primarily to H_2O masers which often have flux densities a few orders of magnitude higher than the weak methanol masers. Therefore, the single HOPS detection at 23.4 GHz towards G357.97−0.16 is not surprising. However, given the typical 5σ noise level and the spectral resolution of HOPS, it seems unlikely that there are many 23.4-GHz masers with a velocity integrated flux density in excess of 4 Jy km s^{-1} (or peak flux density over 10 Jy assuming the same linewidth as in G357.97−0.16).

Interestingly, the relative flux densities of the 25-GHz maser series have the same trend with respect to the quantum number *J* as

in G343.12−0.06, where a number of rare class I methanol masers originate at single location associated with the strong shock traced by H_2 2.12-μm emission (cf. Table 2 in this paper and fig. 5 in Voronkov et al. 2006). In both sources, the maser in the $J = 2$ transition is relatively weak, while all masers corresponding to higher J have comparable flux densities. In addition, both sources have rare 9.9-GHz masers. These similarities encouraged us to search for 23.4-GHz masers towards G343.12−0.06. We examined CABB commissioning data on the source (observed on 2010 June 3, archive project code CX110) and found a 23.4-GHz maser as a single spectral channel spike in the broad-band spectrum which has a velocity resolution of about 13 km s^{-1}. The corresponding velocity integrated flux density was 1.6 ± 0.2 Jy km s^{-1}, which is comparable to the value observed for the 25-GHz masers in the same source (both according to these low-resolution data and to more accurate measurement of Voronkov et al. 2006), and the 9.9-GHz maser is only slightly stronger. Without a zoom window positioned to observe this maser with high velocity resolution, we are unable to quantify its intrinsic peak flux density. However, assuming a spectral profile similar to the 25-GHz masers, the flux density of the 23.4-GHz maser in G343.12−0.06 is expected to be around 7 Jy.

Comparison of the relative integrated flux densities (or peak values) of the 9.9-, 23.4- and 25-GHz masers in G343.12−0.06 and G357.97−0.16 (cf. Table 2 in this paper and table 2 in Voronkov et al. 2006) suggests that there is no linear relation between them. For example, the 23.4- and 25-GHz masers have comparable strength in G343.12−0.06, while the former is notably stronger in G357.97−0.16. Therefore, the new class I maser will provide good constraints for maser models and should be included in future modelling. Further targeted observations, which can be done routinely with a sub-Jy sensitivity at this frequency using ATCA, are required to advance our understanding of the properties of the 23.4-GHz masers. The obvious targets are the known 9.9- and 25-GHz masers.

5 CONCLUSIONS

(i) We report the detection of a new class I methanol maser in the 10_1–9_2 A$^-$ transition at 23.4 GHz. The only HOPS detection of such a maser was towards G357.97−0.16. It was followed up at high angular resolution with ATCA along with the J_2–J_1 E class I methanol maser series. Retrospectively, the 23.4-GHz maser was also found towards G343.12−0.06, another prominent example where rare methanol masers are caused by strong shocks.

(ii) The absolute positions of the 23.4-GHz maser and the 25-GHz maser series coincide within the measurement uncertainty in G357.97−0.16. These masers are located roughly on the extension of the line connecting two known sites of water and 6.7-GHz methanol maser emission, a few arcseconds offset from the southern site. We have detected a weak (1.3 mJy) continuum source associated with the northern site (famous for its water maser with an unusually wide velocity spread). This continuum source may be a hypercompact H II region.

(iii) We report the detection of the 9.9-GHz methanol maser in G357.97−0.16. It is only the fifth maser found in this transition and also has the highest flux density (about 70 Jy) exceeding that of other known 9.9-GHz masers by an order of magnitude.

(iv) High spectral resolution measurement leads us to suggest that the rest frequencies for the $J = 2$, 3 and 4 transitions of the J_2–J_1 E methanol series should be refined to $24\,934.379 \pm 0.001$, $24\,928.7004 \pm 0.0008$ and $24\,933.4698 \pm 0.0008$ MHz, respectively.

ACKNOWLEDGMENTS

The ATCA and the Mopra Telescope are parts of the Australia Telescope National Facility which is funded by the Commonwealth of Australia for operation as a National Facility managed by CSIRO. The University of New South Wales Digital Filter Bank used for the observations with the Mopra Telescope was provided with support from the Australian Research Council. The research has made use of the NASA/IPAC Infrared Science Archive, which is operated by the Jet Propulsion Laboratory, California Institute of Technology, under contract with the National Aeronautics and Space Administration.

REFERENCES

Barrett A. H., Schwartz P. R., Waters J. W., 1971, ApJ, 168, L101
Batrla W., Matthews H. E., Menten K. M., Walmsley C. M., 1987, Nat, 326, 49
Becker R. H., White R. L., Helfand D. J., Zoonematkermani S., 1994, ApJS, 91, 347
Breen S. L., Caswell J. L., Ellingsen S. P., Phillips C. J., 2010, MNRAS, 406, 1487
Caswell J. L., 1998, MNRAS, 297, 215
Caswell J. L. et al., 2010, MNRAS, 404, 1029
Cragg D. M., Johns K. P., Godfrey P. D., Brown R. D., 1992, MNRAS, 259, 203
Cyganowski C. J., Brogan C. L., Hunter T. R., Churchwell E., 2009, ApJ, 702, 1615
De Buizer J. M., Vacca W. D., 2010, AJ, 140, 196
Haschick A. D., Menten K. M., Baan W. A., 1990, ApJ, 354, 556
Hills R., Pankonin V., Landecker T. L., 1975, A&A, 39, 149
Kurtz S., Hofner P., Álvarez C. V., 2004, ApJS, 155, 149
Mehrotra S. C., Dreizler H., Mäder H., 1985, Z. Nat., 40a, 683
Menten K. M., Johnston K. J., Wilson T. L., Walmsley C. M., Mauersberger R., Henkel C., 1985, ApJ, 293, L83
Menten K. M., Walmsley C. M., Henkel C., Wilson T. L., 1986, A&A, 157, 318
Müller H. S. P., Menten K. M., Mäder H., 2004, A&A, 428, 1019
Plambeck R. L., Menten K. M., 1990, ApJ, 364, 555
Slysh V. I., Kalenskii S. V., Val'tts I. E., Otrupcek R., 1994, MNRAS, 268, 464
Sobolev A. M., Ostrovskii A. B., Kirsanova M. S., Shelemei O. V., Voronkov M. A., Malyshev A. V., 2005, in Churchwell E., Conti P., Felli M., eds, Proc. IAU Symp. 227, Massive Star Birth: A Crossroads of Astrophysics. Cambridge Univ. Press, Cambridge, p. 174
Sobolev A. M. et al., 2007, in Chapman J. M., Baan W. A., eds, Proc. IAU Symp. 242, Astrophysical Masers and Their Environments. Cambridge Univ. Press, Cambridge, p. 81
Taylor G. B., Morris M., Schulman E., 1993, AJ, 106, 1978
Voronkov M. A., Sobolev A. M., Ellingsen S. P., Ostrovskii A. B., 2005, MNRAS, 362, 995
Voronkov M. A., Brooks K. J., Sobolev A. M., Ellingsen S. P., Ostrovskii A. B., Caswell J. L., 2006, MNRAS, 373, 411
Voronkov M. A., Brooks K. J., Sobolev A. M., Ellingsen S. P., Ostrovskii A. B., Caswell J. L., 2007, in Chapman J. M., Baan W. A., eds, Proc. IAU Symp. 242, Astrophysical Masers and Their Environments. Cambridge Univ. Press, Cambridge, p. 182
Voronkov M. A., Caswell J. L., Ellingsen S. P., Sobolev A. M., 2010, MNRAS, 405, 2471
Walsh A. J., Lo N., Burton M. G., White G. L., Purcell C. R., Longmore S. N., Phillips C. J., Brooks K. J., 2008, Publ. Astron. Soc. Australia, 25, 105

This paper has been typeset from a TEX/LATEX file prepared by the author.